

Physical Rock Property Constraints and Regional Geophysical Interpretations of the Northeast Thelon Basin, Nunavut

Tschirhart, V. ^[1], Morris, W.A. ^[2], Jefferson, C.W. ^[1]

1. Geological Survey of Canada, Natural Resources Canada, Ottawa, Canada

2. School of Geography & Earth Sciences, McMaster University, Hamilton, Ontario, Canada

ABSTRACT

The northeast Thelon Basin, Nunavut, has been subject to fairly recent and detailed studies as part of the Northern Uranium for Canada project under the Geological Survey of Canada's Geo-mapping for Energy and Minerals program. This project included acquisition of new airborne radiometric and magnetic datasets, compilation of industry airborne magnetic datasets, seven field seasons of bedrock mapping, two field seasons of targeted ground gravity transects, and over 900 density and magnetic susceptibility measurements. Integrating all the available geophysical and geological information produced a remote predictive geological map below the sedimentary cover identifying unconformity-related uranium prospective areas. By linking the rock property information to outcrop and drill core geology and geophysical characteristics it is clear that the diverse magnetic and density characteristics of major rock packages provide quantitative three-dimensional constraints on the distribution of lithological units below sedimentary cover. The maps and interpretations can be used to inform and guide future exploration in the region.

INTRODUCTION

Basin modelling of potential field data has long been employed by the oil and gas industry to generate comprehensive framework geometries of prospective basins. By analyzing the gravity and magnetic data, the company can assess the viability of the basin by mapping fault (trap) locations and depth to basement, while minimizing risk and exploration costs. The reconnaissance knowledge can guide industry towards favourable areas for detailed follow-up. This ideology can be employed to mineral exploration in similar basin settings. Unconformity-related uranium deposits traditionally form in Paleoproterozoic sedimentary basins at the intersection of high angle reactivated faults cross-cutting fertile basement units near the basement-sandstone interface (Jefferson et al., 2007). Thus, a crucial step in understanding the exploration problem is having a sound understanding of the geology, depth to basement, and fault history of the region.

During its >50 year exploration history the Thelon Basin (Figure 1), straddling the border of Northwest Territories and Nunavut, has experienced periodic uranium exploration cycles, resulting in a comprehensive, albeit still poorly constrained geological framework. The majority of deposits and prospects are structurally controlled by multiple intersecting faults interpreted as products of Riedel shear (now recognized by industry operating in the region and the Geological Survey of Canada (GSC)) and hosted in the basement rocks (Figure 1) outside the basin margins. Mineralization along the Kiggavik–Andrew Lake structural trend is also associated with an east-west fault system associated with alteration halos in the Archean supracrustal rocks (Riegler et al., 2016). Demagnetization due to hematitization and clay alteration along structures is visible as non-magnetic lineaments in the magnetic anomaly map

(Tschirhart et al., 2013a). ~80 km north of Kiggavik, sandstone-hosted uranium occurrences within early Paleoproterozoic supracrustal units transecting the central axis of the basin have also been targeted by exploration companies (Figure 1; Miller and LeCheminant, 1985). Within the basin, little knowledge is available regarding the basement geology at or below the unconformity surface. Sparse documented seismic refraction depth estimates and eight boreholes intersect the unconformity surface, the remaining 12 providing minimum geological and depth constraints. Interpretations within the basin are thus heavily reliant on the use of potential field geophysical datasets (Tschirhart et al., 2014).

Key to understanding the uranium potential within the Thelon Basin is the geology and structure of the underlying supracrustal belts and intrusive suites that are buried under sedimentary cover. Geophysical anomaly patterns and their signal attributes, analyzed in the context of rock properties, must be used to discriminate the buried units. These can also define important exploration parameters for unconformity-related uranium deposits, such as reactivated faults and fertile basement supracrustal belts. This contribution provides a case study of the utility of physical rock property information for assisting in such regional geophysical-geological interpretations.

GEOLOGICAL SETTING

The Thelon Basin is an intracratonic basin covering ~85 000 km² located in the Rae craton of the western Churchill Structural Province. Filled by flat-lying siliciclastic sedimentary sequences of the Thelon Formation, the basin was predated by the 1.83 Ga Hudsonian Orogeny (Van Breemen et al. 2005; Pehrsson et al. 2013) and the 1.75 Ga Kivalliq igneous event (Peterson et al. 2015a).

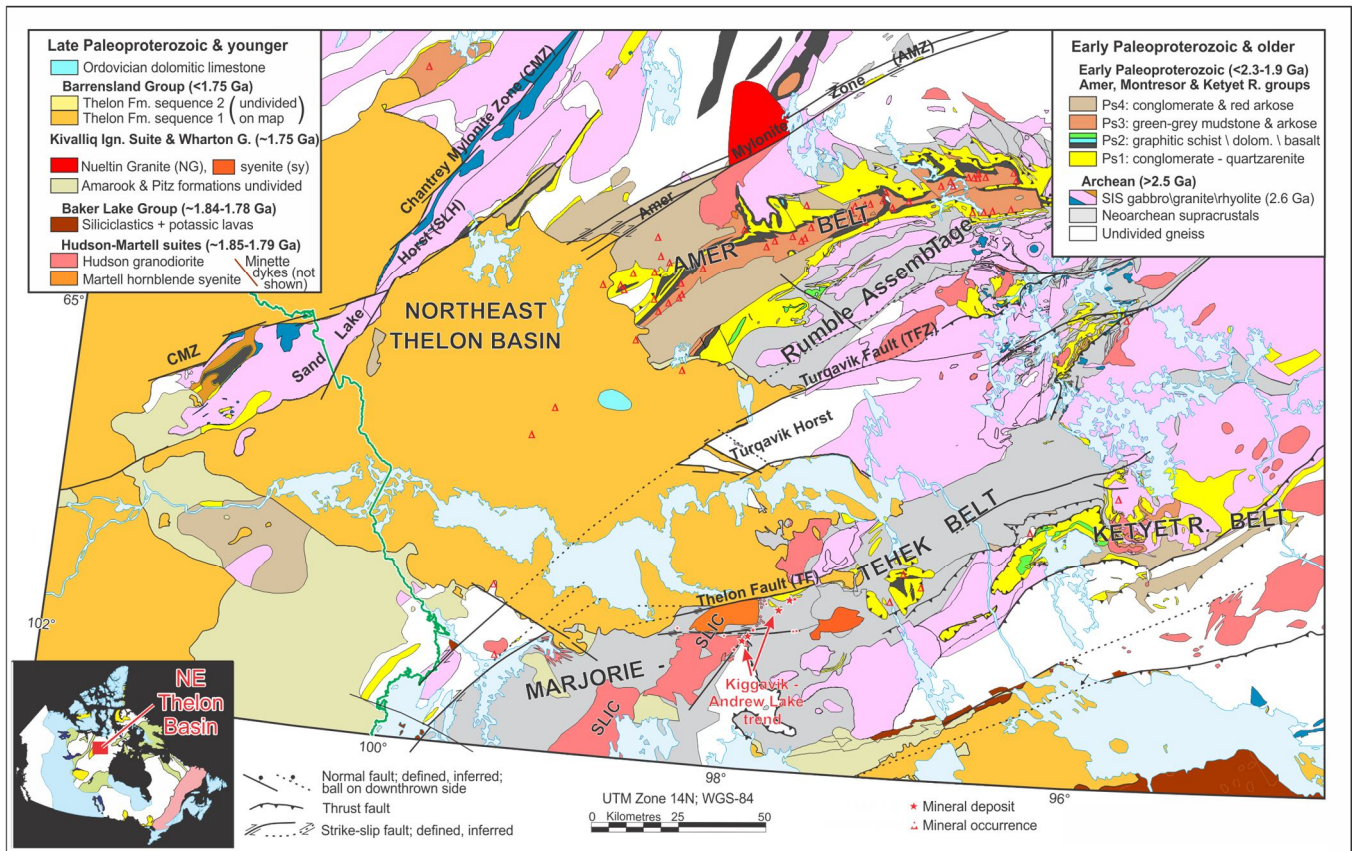


Figure 1: Generalized geological map of the northeast Thelon Basin (after Jefferson et al., 2015; from Tschirhart et al., 2017).

The Thelon Formation is a remnant of a huge sand sheet that unconformably overlies the 1.75 Ga Wharton Group and bimodal intrusions of the Kivalliq igneous suite, the 1.83 Ga Baker Lake Group and Hudson intrusive suite, Paleoproterozoic strata of the Amer, Ketyet River and Montesor belts, 2.6 Ga bimodal igneous rocks of the Snow Island suite, the ~2.61 Ga Marjorie Hills assemblage (MHA), >2.63 Ga supracrustal assemblages of the Woodburn Lake group, e.g. the Rumble assemblage (RA), and poorly known Archean gneissic rocks. Sedimentation of the Thelon Formation post-dated the Kivalliq igneous suite and was punctuated by 1.67 Ga uranium-bearing fluorapatite cementation which also records hydrothermal mobilization of uranium (Davis et al., 2011). These packages are cross-cut by strike-slip and dip-slip faults that were reactivated periodically from ~1.83 Ga to recent times. Multiple, moderately magnetic dyke swarms, partial products of the 1.75 and 1.83 Ga magmatic events, as well as the strongly magnetic 1.27 Ga Mackenzie dykes, are spatially associated with the reactivated fault arrays.

GEOPHYSICAL DATASETS

Magnetics

Aeromagnetic datasets available over the northeast Thelon Basin (Tschirhart et al., 2011) include eight industry surveys of

variable orientation and line spacing, three 400 m-line spaced surveys acquired by the Geological Survey of Canada (GSC) and regional 805 m-line spaced surveys acquired by Natural Resources Canada in the 1970s. The industry and GSC surveys were upward continued to a common flight elevation of 150 m, merged to create a contiguous compilation grid, and reduced-to-pole (Figure 2). Subsequent data processing was performed on this composite grid.

Gravity

Regional ground gravity stations are spaced 10–15 km apart and are available from the Canadian Gravity Database. Fieldwork conducted during the summers of 2010 and 2011 acquired additional ground gravity data along transects across key geophysical and geological features, and provide additional parameters to constrain the subsurface geometry (Tschirhart et al., 2013, 2016). The ground gravity data were corrected for latitude, instrument drift, elevation, and Earth's tides, followed by application of the Free Air and Bouguer corrections. The data were reduced to a Bouguer slab density of 2.67 g/cm³ and no terrain corrections were made in light of minor elevation differences across the area.

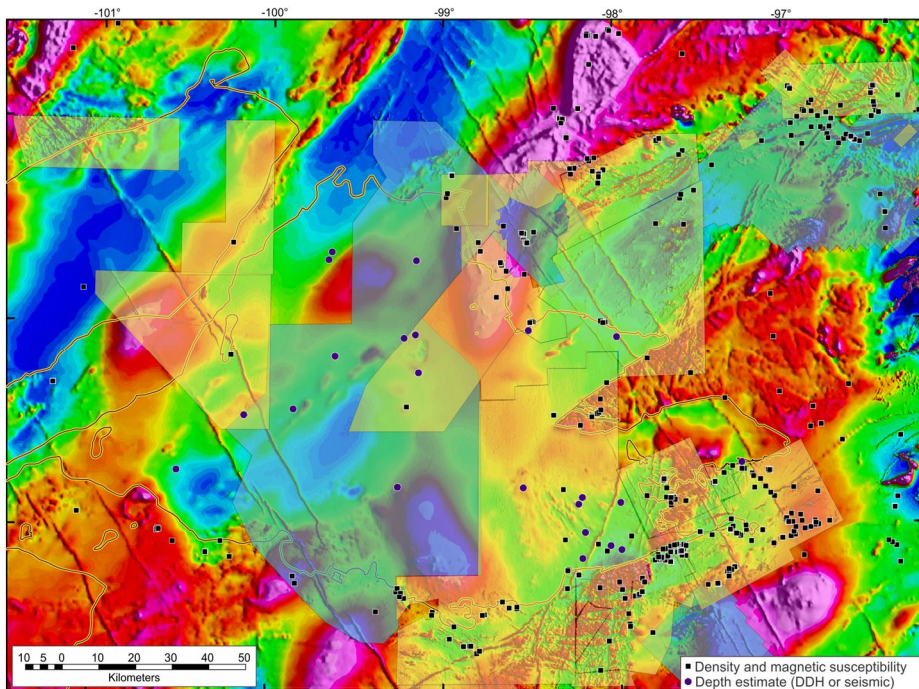


Figure 2: Field data locations on merged reduced-to-pole magnetic grid over the northeast Thelon Basin (outlined in yellow). Transparent yellow polygons represent industry aeromagnetic surveys; blue polygons represent GSC surveys.

Rock Properties

Rock samples collected during the 2007–2011 field seasons were selected to represent the range of rock units encountered in the area and to provide density and magnetization constraints for modelling (Figure 2, Table 1; Tschirhart et al., 2013, 2016). Remanence information was not available. Magnetic susceptibility values were measured using a KT-10 magnetic susceptibility meter. Density was measured using the Archimedes submersion approach. The heterogeneous lithology of many of the map units, together with variable levels of alteration, resulted in wide range of physical property values summarized in Table 1 (from Tschirhart et al., 2017).

Data Processing

Within the interior of the northeast Thelon Basin it is difficult to trace the exact extents of lithological units as the observed magnetic signal is attenuated with increasing distance from source to sensor as sedimentary cover thickens. Source edge detection (SED) techniques have been employed to enhance the edges of magnetic sources. SED techniques maximize some function over the edge or centre of a magnetic body, provided there is sufficient contrast between the magnetic susceptibilities of laterally adjacent units. Pilkington and Keating (2009) compare and contrast a variety of techniques concluding no single technique on its own is better than the others in all geological circumstances. Using the reduced-to-pole merged magnetic field grid, we chose to use the normalized tilt derivative (TDX; Cooper and Cowan, 2006) displayed with transparency over the Theta map (Wijins, 2005). Normalizing techniques have the advantage of enhancing sources located at

depth and at surface equally and were helpful in identifying compositional variations in the broad magnetic bodies. In such cases, multiple anomalies from various depths and magnetizations produce the observed signal.

The depth extent of the sedimentary infill and underlying supracrustal units, and fault morphology were interpreted from semi-automated depth estimation techniques and modelling described in Tschirhart et al., (2014). Geological and physical property data informed the choice of depth estimation technique and parameters (structural index, constraints). For example, outcrop mapping by Jefferson et al. (2015) defines many sources that can be approximated by discrete 2D magnetic sources and are suitable candidates for simple parametric inversions. Using the semi-automated depth algorithms, large anomalies correlated to plutonic intrusions were interpreted with a different structural index ($SI = 0$) than a thin, dyke-like body ($SI = 1$) such as the Ps2 and Ps3 anomalies. Additionally, knowledge of the variable magnetization of bimodal volcanic rocks from magnetic susceptibility measurements (Kivalliq igneous suite in Table 1) guided the interpretation in some regions, whereby the minimum depth estimates may represent the uppermost flows. Stacking of multiple solutions across depth estimation techniques further increased the confidence of the interpretation.

PREVIOUS GEOPHYSICAL STUDIES

Prior to undertaking regional geological-geophysical interpretations (Tschirhart et al., 2014, 2017), a series of papers were published by the authors detailing geophysical modelling results over key litho-structural entities that were constrained by density and magnetic susceptibility information (Tschirhart et al., 2013a, b), and are summarized below. Together with bedrock mapping (Jefferson et al., 2015), the rock property characteristics (Table 1) and modelled structural styles informed the interpretations of the authors in understanding the regional geological setting below sedimentary cover.

The authors identified discrete magnetic stratigraphic horizons in the Amer Belt (Figure 1; Ps2 Five Mile Lake formation basalt; Ps3 Three Lakes formation mudstone and siltstone; and Ps3 Showing Lake formation mudstone and sandstone), a wedge-shaped multiply deformed belt that transects the central axis of the basin (Tschirhart et al., 2013b). Tschirhart et al. (2013b) forward and inverse modelled the east-northeast portion of this belt as an open, doubly plunging syncline cored by Ps4 unconformably overlying a previously folded and imbricated complex of Ps1–3 units. The strong magnetization in the Ps3 metasedimentary units is caused by sedimentary layers rich in disseminated euhedral magnetite that generate several discrete

linear marker units that can be traced along the length of the fold belt. Around the Kiggavik region (Figure 1), the authors characterized the non-magnetic, moderately dense metasedimentary Archean basement (MHA vs. Woodburn Lake group; Tschirhart et al., 2013a) and defined the geometry of the variably magnetic 1.83 Ga plutonic bodies, one of which they modelled as thick sills within the MHA thrust over the Woodburn Lake group.

MAGNETIC CHARACTERISTICS

Rock properties provide the fundamental link between the geophysical signature and the subsurface geology. Within the study area, many lithological units can be distinguished by their magnetization and density characteristics, which provide constraints to guide the interpretation process at a variety of scales. Table 1 shows the distribution of high versus low magnetic susceptibility populations. In addition to the metasedimentary and intrusive units discussed above, several other strongly magnetic units punctuate the magnetic field grid (after Tschirhart et al., 2017; Table 1; Figure 2). Large deep plutons of the 2.6 Ga Snow Island suite (Peterson et al. 2015c)

form pronounced, broad 25–40 km circular to elliptical anomalies 300–600 nT and are the largest anomalies in the study area (Figure 3 – SIS). Circular magnetic anomalies 6–10 km in diameter cored by non-magnetic rocks were identified by the authors south of the study area corresponding to 1.76 Ga Nueltin intrusions (Peterson et al., 2015a, 2015b). Similar anomalies were identified adjacent to and within the Thelon Basin (Figure 3 – Nlt), with the anomalies adjacent to the basin corroborated by bedrock mapping observations. The magnetically dappled Turqavik Horst (Figure 3 - Tur) is truncated on the northern flank by the Turqavik fault zone (TFZ), and can be easily traced below the sedimentary cover. Mottled magnetic textures along the southern margins of the basin are correlated to bimodal volcanic rocks of the Pitz Formation (Figure 3 – Pitz; Tschirhart et al., 2014). Northeast trending 1.6–2 km wide oblong magnetic anomalies are located below the metasedimentary belts (Figure 3 – M; Tschirhart et al. 2014) and are interpreted to represent mafic to ultramafic intrusions that are focused along the Amer Mylonite Zone, and are interpreted to underlie Amer Group supracrustal rocks.

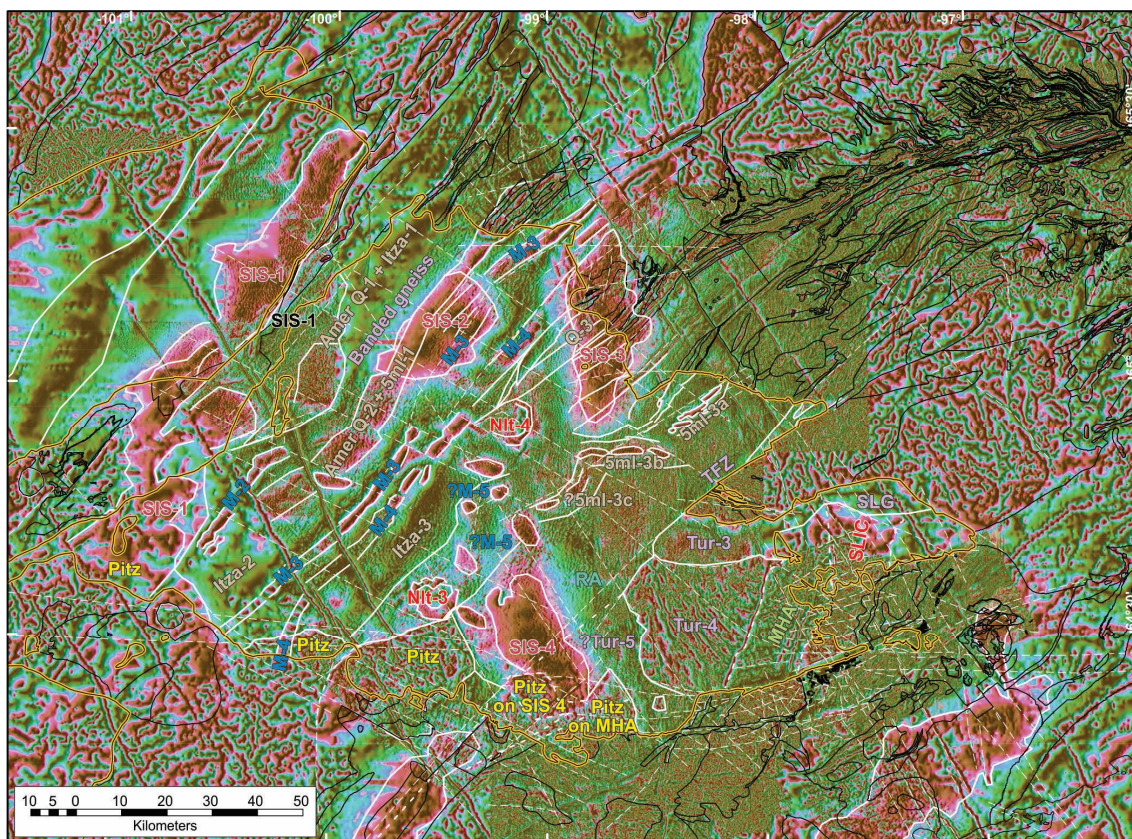


Figure 3: TDX grid 60% transparency over greyscale Theta grid. The outline of the Aberdeen sub-basin and previously mapped geological contacts and labels outside of it are in black (after Jefferson et al. 2015). Newly mapped geophysical units outlined in white are labelled as discussed in the text and as follows: 5ml – Five Mile Lake formation; Itza – Itza lake formation; Amer Q – Ayagaq lake formation. From Tschirhart et al. 2017.

The least magnetic rocks as detailed in Table 1 comprise the unconformably overlying Thelon Formation, Amarook Formation of the Wharton Group, Ps1 Ayagaq lake formation and much of the Ps4 Itza lake formation of the Amer Group, metagreywacke of the Woodburn Lake group and the MHA (excluding the Archean iron formations and upper Itza lake formation linear magnetic markers that resemble those of the Montresor Belt). Magnetically, these units are virtually indistinguishable from each other; however, as noted in Table 1 they have varying density characteristics. The density information was used to constrain gravity forward models in Tschirhart et al. (2017).

GEOLOGICAL INTERPRETATION

The above geophysical data and properties were used to extrapolate the limited outcrop geological data and build the regional predictive map shown in Figure 4a. Where there is no sharp contrast in magnetization, the shape, texture, structural style and continuity of a magnetic anomaly from exposed basement constrains what lithological units the anomaly might represent. Truncations, discontinuities and displacement of magnetic marker units on the SED images were interpreted as faults in addition to traditional identification of faults from air photos, digital elevation models and geological mapping (Jefferson et al., 2015; Tschirhart et al., 2017) and plotted as lines in Figure 4a.

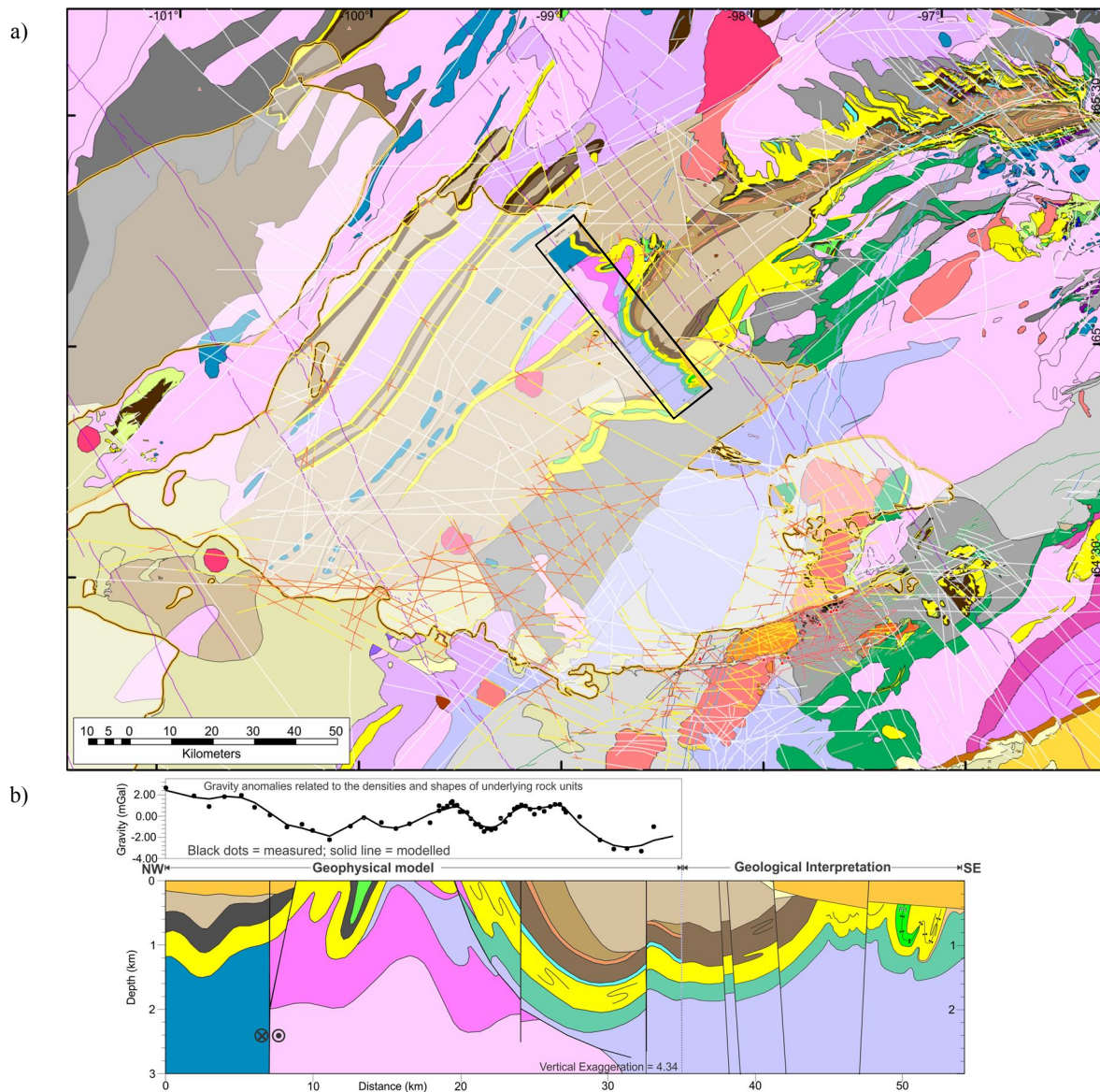


Figure 4: (a) Remote predictive map of the geology at the unconformity surface. Surrounding geology is after Jefferson et al. (2015). Outline of Thelon Formation is shown by thin black line on thick orange line. White lines are selected reactivated faults, yellow lines are reactivated faults within fertile basement units, and red lines are intersecting reactivated faults in fertile basement units. (b) Forward gravity model with geological interpretation to the southeast. Forward model plotted on (a). Colours as in Figure 1. From Tschirhart et al. 2017.

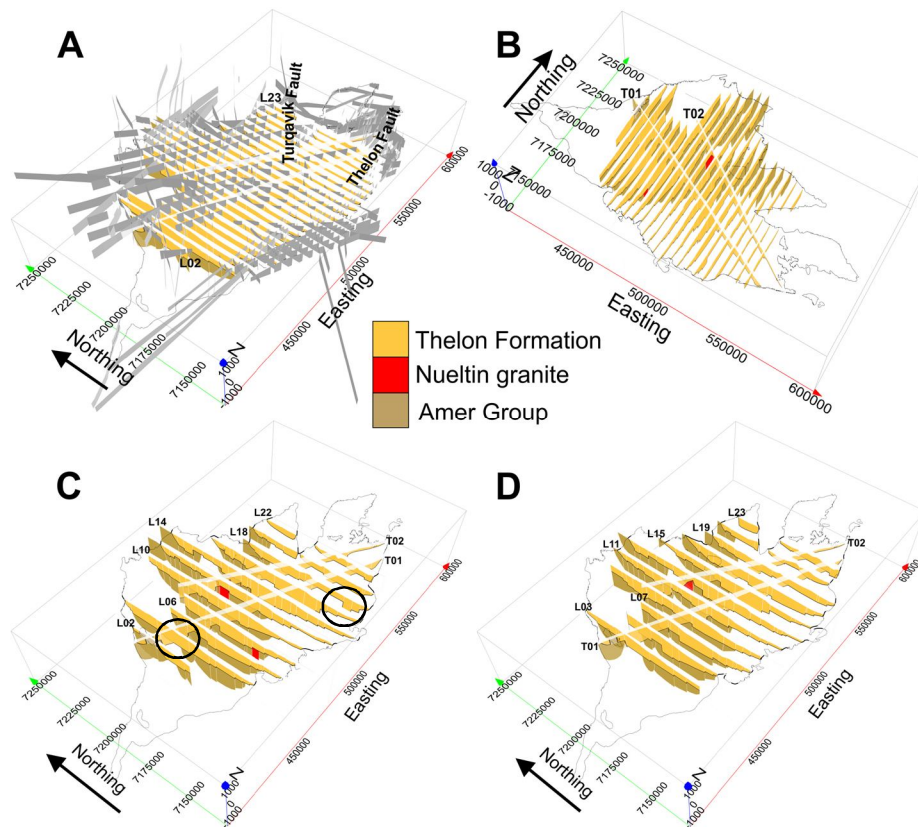


Figure 5: (a) Pseudo 3D model of the northeast Thelon Basin showing all constructed cross-sections. Fault surfaces shown in grey, outline of the northeast Thelon Basin surface shown in black and cross-sections labelled; (b) All constructed cross-sections; (c) Odd numbered cross-sections; (d) Even numbered cross-sections. Vertical exaggeration = 15. From Tschirhart et al. (2014). Deepest locations labelled by black circles.

In addition to gravity modelling products produced for the northeast Amer Belt (Tschirhart et al., 2013b) and the Kiggavik region (Tschirhart et al., 2013a), four gravity forward models constrained by density information describe the structural style of the Amer Belt within the basin, and are in general agreement with the structural style documented in the northeast (Tschirhart et al., 2013b). Furthermore, the remote predictive maps show the southwest end of the Amer Group as two broad synclines separated by an axial anticline (cross-section in Figure 4b).

PSEUDO 3D MODELLING

Following the first iteration of the remote predictive map, Tschirhart et al. (2014) constructed a pseudo 3D model along a series of transects cross-cutting the basin, modelling the thickness of the sedimentary cover and underlying supracrustal units (Figure 5). Previously mapped faults transecting the northeast Thelon Basin were assigned a down-drop direction based on the apparent throw of the magnetic unit (Tschirhart et al., 2014), and depth to magnetic source was estimated using a variety of depth estimation techniques taking into account the geometry and magnetization characteristics discussed above (Table 1), and incorporating ‘hard constraints’ where available. The process is described in detail in Tschirhart et al. (2014). The northeast Thelon Basin was modelled with a highly variable

basement topography, with the deepest regions located at ?Tur-5 and Itza-2 (Figure 4 – black circles). Both areas are bounded by faults with a pronounced down-drop and display little magnetic character. The northwest-southeast fault system, termed the Mackenzie fault array by Tschirhart et al. (2014) (and Bathurst fault array in Tschirhart et al. 2017) appears to be the most dominant structural array controlling the geometry (and depth) of the basin.

DISCUSSION

Confidence in the remote predictive mapping of basement beneath the northeast Thelon Basin is high where there is minimal sedimentary cover, there is agreement with modelled gravity data, and where exposed features can be tracked for large distances. This is especially true of features with distinctive magnetic characteristics such as the Nueltin intrusions (Peterson et al., 2015a), the Turqavik Horst, and Snow Island suite (Peterson et al., 2015c; Figures 3 and 4).

Using the interpreted basement geology and mapped or inferred faults, prospective fault intersections can be highlighted. In the Kiggavik area reactivated faults are critical especially where they intersect. Uranium was transported through reactivated fault zones by oxidized hydrothermal fluids and reduced at

REFERENCES

hydrogeological focus points to allow deposition of uranium oxide minerals with concomitant production of iron oxide from mafic and sulphide minerals in the faulted and fractured host rocks (Jefferson et al. 2007). The analogy beneath the northeast Thelon Basin is graphitic units within Ps2 that flank the Ps1 Ayagaq Lake quartzite; however, these are non-magnetic and are not visible on the aeromagnetic imagery and not interpreted here. It is also possible that stratabound sandstone hosted uranium pods within magnetic Ps3 Showing lake formation may have been re-concentrated by unconformity-related hydrothermal processes. As such, reactivated intersections of the four main late brittle regional fault arrays within fertile basement (i.e. those with favourable lithology or potential uranium-rich source rocks) such as Showing lake formation, MHA, RA and Nueltin granite, are key foci in the search for unconformity-related uranium deposits. These areas beneath the northeast Thelon Basin are labelled by red lines in Figure 4a.

In targeting unconformity related uranium, depth to basement must also be considered for accessing the economic viability. Favourable intersections (fertile units with cross-cutting, intersecting faults; Figure 4 – red lines) located under more than a few 100 m of strata may not be a suitable exploration target. Tschirhart et al. (2014)'s pseudo 3D modelling of the sedimentary cover and supracrustal units provides a first order model when looking at the depth to basement.

The next step in assessing the regional uranium prospectivity of the basin is generating an integrated model that combines the depth to basement information with the predictive geological map and favourable fault intersections. However, given the current state of exploration (or lack thereof) in the Thelon Basin, this is not of immediate concern.

CONCLUSIONS

In the absence of rock property and geological information the geophysical signature is inherently non-unique and cannot be accurately tied to the surface geology in the absence of a prior information. Rock property datasets provided vital information for regional geological-geophysical interpretations in this remote region to generate the first-ever remote predictive basement geological map for the northeast Thelon Basin. The new map and pseudo 3D model provide a knowledge framework for developing future exploration programs and a platform for testing evolving geological interpretations as future exploration programs generate higher resolution data that can provide additional constraints. Advanced drill programs and subsurface geophysical investigation can test and build on this contribution to further improve the knowledge infrastructure.

ACKNOWLEDGEMENTS

This paper integrates results from five papers published as part of the first author's PhD thesis. Reviews by Mark Pilkington greatly improved the quality of the manuscript.

Cooper G.R.J. and D.R. Cowan, 2006, Enhancing potential field data using filters based on the local phase: *Computers and Geosciences*, 32, 1585–1591.

Davis, W.J., Q. Gall, C.W. Jefferson and R.H. Rainbird, 2011, Diagenetic fluorapatite in the Paleoproterozoic Thelon Basin: structural-stratigraphic context, in situ ion microprobe U-Pb ages and fluid flow history: *Bulletin of the Geological Society of America*, 123, 1056–1073.

Jefferson, C. W., D. Thomas, D. Quirt, C.J. Mwenifumbo, and D. Brisbin, 2007, Empirical models for Canadian unconformity associated uranium deposits, in B. Milkereit ed., *Proceedings of Exploration 07*, 741-769.

Jefferson, C.W., J.C. White, G.M. Young, J. Patterson, V. Tschirhart, S.J. Pehrsson, L. Calhoun, R.H. Rainbird, T.D. Peterson, W.J. Davis, S. Tella, L.B. Chorlton, J.M.J. Scott, J.A. Percival, W.A. Morris, P. Keating, A. Anand, Y. Shelat, and D. MacIsaac, 2015, Outcrop and remote predictive geology of the Amer Belt and basement beside and beneath the northeast Thelon Basin, in parts of NTS 66-A, B, C, F, G and H, Kivalliq Region, Nunavut: Geological Survey of Canada, Open File 7242, 1 sheet.

Miller A.R. and LeCheminant A.N. 1985. Geology and uranium metallogeny of Proterozoic supracrustal successions, central District of Keewatin, N.W.T. with comparisons to northern Saskatchewan, in T.I.I. Sibbald and W. Petruk, *Geology of Uranium Deposits*, 32, 167–185.

Pehrsson, S.J., R. Berman, and W.J. Davis, 2013, Paleoproterozoic orogenesis during Nuna aggregation: a case study of reworking of the Archean Rae craton, Woodburn Lake, Nunavut: *Precambrian Research*, 232, 167-188.

Peterson, T.D., J.M.J. Scott, A.N. LeCheminant, C.W. Jefferson, and S.J. Pehrsson, 2015a, The Kivalliq Igneous Suite: Anorogenic bimodal magmatism at 1.75 Ga in the western Churchill Province, Canada: *Precambrian Research* 262, 101-119.

Peterson, T.D., J.M.J. Scott, A.N. LeCheminant, V. Tschirhart, L.B. Chorlton, W.J. Davis, and M. Hamilton, 2015b, Nueltin granites and mafic rocks in the Tebesjuak Lake map area, Nunavut: new geochronological, petrological, and geophysical data: *Geological Survey of Canada, Current Research* 2015-5; 23 p.

Peterson T.D., C.W. Jefferson and A. Anand, 2015c, Geological setting and geochemistry of the ca. 2.6 Ga Snow Island Suite in the Central Rae Domain of the Western Churchill Province, Nunavut: *Geological Survey of Canada, Open File* 7841, 29 p.

Pilkington M. and P.B. Keating, 2009, The utility of potential field enhancements for remote predictive mapping: *Canadian Journal of Remote Sensing* 35, S1–S11.

Riegler, T., D. Quirt, and D. Beaufort, 2016, Spatial distribution

and compositional variation of APS minerals related to uranium deposits in the Kiggavik-Andrew Lake structural trend, Nunavut, Canada. *Mineralium Deposita*, 51, 219–236.

Tschirhart V., W.A. Morris and D. Oneschuk, 2011, Geophysical Series, Geophysical Compilation Project, Thelon Basin, Nunavut, NTS 66A, B, and Parts of 65N, O, P, 66C, F, G and H: Geological Survey of Canada, Open File 6944.

Tschirhart, V., W.A. Morris, C.W. Jefferson, 2013a, Framework geophysical modelling of granitoid vs. supracrustal basement to the northeast Thelon Basin around the Kiggavik uranium camp, Nunavut: *Canadian Journal of Earth Sciences*, 50, 667-677.

Tschirhart, V., W.A. Morris, C.W. Jefferson, Keating, P., White, J.C. and Calhoun, L., 2013b, 3D geophysical inversions of the north-east Amer Belt and their relationship to geologic structure: *Geophysical Prospecting*, 61, 547-560.

Tschirhart, V., 2014, Geophysical and geological integration and interpretation of the northeast Thelon Basin, Nunavut: PhD Thesis, McMaster University.

Tschirhart, V., W.A. Morris, and C.W. Jefferson, 2014, Unconformity surface architecture of the northeast Thelon Basin, Nunavut, derived from integration of magnetic source depth estimates: *Interpretation*, 2, SJ263-SJ278.

Tschirhart, V., C.W. Jefferson, and W.A. Morris, 2017, Basement geology beneath the northeast Thelon Basin, Nunavut: insights from integrating new gravity, magnetic and geological data: *Geophysical Prospecting*, 65, 617-636.

Van Breemen, O., T.D. Peterson, and H.A. Sandeman, 2005, U–Pb zircon geochronology and Nd isotope geochemistry of Proterozoic granitoids in the western Churchill Province: intrusive age pattern and Archean source domains *Canadian Journal of Earth Sciences*, 42, 339–377

Wijins C., C. Perez and P. Kowalczyk, 2005, Theta map: Edge detection for magnetic data: *Geophysics*, 70, L39–L43.

Table 1: Modified from Tschirhart et al., (2017). *notes: 1) dykes are defined by orientation and strength of linear magnetic anomaly; 2) underlying markers are subdued in intensity; 3) The only large body in the study area is on the north side of the Amer Mylonite Zone; 4) subtle pattern noted in places south of Aberdeen Lake; 5) mainly in the Schultz Lake Intrusive Suite (SLIC); 6) demagnetization records hydrothermal alteration to hematite and/or clay in linear zones along reactivated steep faults, most evident in thin magnetic units; 7) regionally continuous distinct stratigraphic-structural marker; 8) provides contrast to 7; 9) low magnetic susceptibility but good conductors provide local stratigraphic-structural markers; 10) deep plutons not affected by demagnetization along faults, however in places form lenses along ancient shear zones; 11) BIF is locally the highest contrast marker in several greywacke units; 12) indistinct, in places forms crude linear trend; n) non-diagnostic. Abbreviations in this table and in the figures, in alphabetical order: Avg. = average; BIF = banded iron formation; bslt = basalt; fm. = informal stratigraphic formation name; Ga = billion years; hi = high; lk. = Lake; mag. = magnetic susceptibility; mod. = moderate; n = number of samples measured; na = not applicable; Susc. = magnetic susceptibility

Group / Suite	Map Unit	Map Code	Lithology	Magnetic susceptibility traits	*	Average Susc. (SI)	Average Susc. (log10)	Min.	Max.	Density Avg. g/cc	n
Mackenzie	Mackenzie diabase	Mck-dy	diabase	high, 150° straight	1	0.030280	0.030280	n/a	n/a	3.04	1
Event	(1.17 Ga)	Mck-dy-clay	altered diabase	na	n	0.000034	0.000300	n/a	n/a	2.52	1
Barrenland	Thelon	Th2-cg	conglomerate	non-magnetic	2	0.000018	0.000004	0.000000	0.000043	2.59	4
Group	Formation	Th1-slt	siltstone	non-magnetic	2	0.000007	0.000002	0.000000	0.000014	2.58	4
(<1.75 Ga)	(apatite cement	Th1-ss	sandstone	non-magnetic	2	0.000008	0.000000	0.000000	0.000009	2.48	12
	1.68 Ga)	Th1-cg-sil	interbedded	non-magnetic	2	0.000003	0.000001	0.000000	0.000009	2.62	5
		Th1-cg	conglomerate	non-magnetic	2	0.000034	0.000021	0.000004	0.000137	2.64	18
Kivalliq igneous suite	Nueltin granite	Nlt-gr	granite	high to low areal	3	0.002047	0.000234	0.000000	0.012343	2.63	27
intrusive	Thelon diabase	Th1-dy	diabase	mod.-hi, 075° straight	1	0.027399	0.025958	0.025897	0.026020	2.92	2
components	McRae Lake diabase	McR-dy	diabase	hi, 350-020° straight	1	0.030229	0.023206	0.010857	0.049600	2.80	2
Wharton	Pitz Formation	Pitz-rhy	rhyolite	variable, stippled	4	0.002347	0.000091	0.000017	0.026250	2.63	12
Group	Amarook Fm.	Wh-Ak-cg	conglomerate	non-magnetic	2	0.000043	0.000016	0.000002	0.000206	2.54	9
(1.75 Ga)		Wh-Ak-qz	quartzarenite	non-magnetic	2	0.000014	0.000011	0.000004	0.000034	2.56	5
Hudson	Bostonite dyke	Bstn-dy	fine syenite	mod., 000+125° straight	1	0.000880	0.000254	0.000013	0.002559	2.65	11
Suite	Lamprophyre dyke	Mntt-dy	lamprophyre	mod., 000+125° straight	1	0.000172	0.000099	0.000010	0.000513	2.71	6
(intrusive)	Martell syenite	Mrt-sy (SLIC)	coarse syenite	high, reticulate area	5	0.002003	0.000762	0.000000	0.014360	2.77	7
(1.83 Ga)		Mrt-sy-clay	altered syenite	demagnetized faults	6	0.000022	0.000022	0.000020	0.000024	2.50	2
	Hudson granite	Hds-gr (SLIC)	granodiorite	moderate-high, reticulate	5	0.001785	0.000290	0.000007	0.012640	2.63	38
		Hds-gr-clay	altered granodiorite	demagnetized faults	6	0.000004	0.000003	0.000001	0.000008	2.42	4
		Hds-peg	pegmatite	na	n	0.000103	0.000052	0.000014	0.000193	2.60	2
Amer Group	Ps4: Itza Lake fm.	Itz-fss	arkosic sandstone	low	2	0.000053	0.000023	0.000001	0.000298	2.64	26
(all	< 1.91 Ga	Itz-fmd	red mudstone	low	2	0.000109	0.000080	0.000012	0.000272	2.70	8
formation	Ps3: Showing lk. fm.	Shw-fsmd	mudstone & siltstone	high, folded linear	7	0.001444	0.000167	0.000015	0.014733	2.76	22
names	Ps3: Oora lk. fm.	Orl-fss	feldspathic sandstone	low	8	0.000345	0.000196	0.000042	0.000966	2.62	11
(fm.) are informal	Ps3: Three Lakes fm.	3lk-md	grey mudstone & siltstone	high, folded linear	7	0.004215	0.000480	0.000058	0.020627	2.78	7
	Ps2: Five Mile lk. bsl.	5ml-v	porphyritic basalt	high, curvilinear	7	0.007219	0.000890	0.000003	0.054617	2.86	31
	Ps2: Aluminium R. fm.	Alm-dol	siliceous dolostone	low	8	0.000035	0.000021	0.000004	0.093010	2.81	14
	Ps2: Resort lk. fm.	Rsl-fqz	feldspathic sandstone	low	8	0.000067	0.000040	0.000004	0.000215	2.71	17
	(<1.95 Ga)	Rsl-mdsl	graphitic meta-mudstone	low but with conductors	9	0.000285	0.000090	0.000000	0.002265	2.75	40
	Ps1: Ayagaq lk. fm.	Ayg-qzp	pyritic quartzite	low	8	0.000030	0.000012	0.000003	0.000084	2.67	5
	(<<2.3 Ga)	Ayg-cgu	conglomerate	low	8	0.000060	0.000007	0.000000	0.000155	2.70	12
		Ayg-qzar	quartzarenite	low	8	0.000060	0.000018	0.000001	0.000513	2.68	19
		Ayg-srqs	sericitic quartzite	low	8	0.000240	0.000056	0.000010	0.001048	2.78	7
Marjorie Hills assemblage		MI-BIF	clay altered metagreywacke	very high, folded linear	11	0.000046	0.000045	0.000036	0.000055	2.95	2
(informal)		MI-gw	metagreywacke, thick beds	low to moderate, areal	n	0.000458	0.000089	0.000001	0.004217	2.68	17
(<2.63 Ga, V.McNicoll, personal		MI-gw-hem	metagreywacke, hematitized	demagnetized	6	0.000012	0.000007	0.000037	0.000218	2.65	3
communication, March 2013)		MI-fv	felsic metavolcanic rock	na	n	0.004344	0.001294	0.000362	0.010081	2.79	4
		MI-mv	mafic metavolcanic rock	moderate-high, broad	12	0.028647	0.006921	0.000030	0.093107	2.93	6
Snow Island	mafic intrusions	Snw-di, -gb	diorite to gabbro	high, strong peaks	10	0.000260	0.000030	0.000000	0.000446	2.79	3
Suite (SIS)	granitoid rocks	Snw-mzdi	grano- to monzodiorite	moderate-high, domal	10	0.003260	0.000230	0.000005	0.015647	2.69	5
(2.6 Ga)	volcanic rocks	Snw-rhy	qtz-fsp porphyritic tuff	low	n	0.000213	0.000044	0.000007	0.003643	2.66	34
Woodburn	Pipedream	Ppd-BIF	chert-magnetite BIF	very high, folded linear	11	0.030897	0.002414	0.000046	0.164610	3.04	12
Lake	assemblage	Ppd-clay	clay altered greywacke	demagnetized	6	0.000004	0.000004	n/a	n/a	2.31	1
group	(informal)	Ppd-fv	felsic metavolcanic rock	na	n	0.000094	0.000046	0.000006	0.000179	2.70	13
	(<2.71 Ga)	Ppd-gw	metagreywacke, thin beds	weak	n	0.000509	0.000092	0.000000	0.008549	2.70	83
		Ppd-gw-clay	clay altered metagreywacke	demagnetized faults	6	0.000018	0.000013	0.000006	0.000043	2.49	5
	These values apply to	Ppd-gw-hem	metagreywacke, hematitized	demagnetized faults	6	0.000215	0.000043	0.000005	0.000613	2.69	3
	other assemblages in	Ppd-mv	metagreywacke, hematitized	low	12	0.000245	0.000244	0.000036	0.000265	2.95	2
	study area, e.g. the	Ppd-md	graphitic meta-mudstone	low (locally conductive)	9	0.000055	0.000029	0.000008	0.000137	2.75	3
	Turqavik Belt	Ppd-qz	thin yellowish quartzite	na	n	0.000009	0.000004	0.000000	0.000061	2.65	13
Undivided	Granitoid gneiss	A-gtoid	granitic gneiss	moderate, areal	n	0.000778	0.000268	0.000015	0.006456	2.72	14
Archean		A-gtoid-clay	clay altered gneiss	non-magnetic	6	0.000005	0.000005	n/a	n/a	2.52	1
basement	Felsic metavolcanic	A-fv	felsic metavolcanic rock	low to moderate	n	0.002481	0.000035	0.000035	0.011587	2.72	13
	Mafic metavolcanic	A-mv	mafic metavolcanic rock	moderate-high, broad	12	0.000425	0.000320	0.000068	0.001436	2.82	14